12

Aging-Induced, Defect-Mediated Double Ferroelectric Hysteresis Loops and Large Recoverable Electrostrain Curves in Mn-Doped Orthorhombic $KNbO_3$-Based Lead-Free Ceramics

Siu Wing Or
Department of Electrical Engineering, The Hong Kong Polytechnic University, Hung Hom, Kolwoon, Hong Kong

1. Introduction

Aging is a physical phenomenon in many ferroelectric materials characterized by the spontaneous changes of dielectric, ferroelectric, and piezoelectric properties with time (Jaffe et al., 1971; Lambeek & Jonker, 1986; Schulze & Ogino, 1988; Uchino, 2000). Aging is generally considered to be detrimental because it tends to limit the application viability of ferroelectric materials in terms of reliability and stability. Recently, a series of studies show that aging is useful and valuable to intensionally induce anomalous double (or constricted) ferroelectric hysteresis (P–E) loops, and hence large recoverable electrostrain (S–E) curves, in impurity- or acceptor-doped tetragonal ferroelectric titanates, such as barium titanate ($BaTiO_3$) (Lambeek & Jonker, 1986; Ren, 2004; Zhang & Ren, 2005; Zhang & Ren, 2006). Specifically, these aging effects can provide an alternative way of both physical interest and technological importance to modify or enhance the electromechanical properties of tetragonal ferroelectrics. From the phenomenological respects, the aging effects can be described by a gradual stabilization of ferroelectric domain structure by defects (i.e., dopant, vacancy or impurity) (Arlt & Rebels, 1993; Damjanovic, 1998; Hall & Ben-Omran, 1998). In fact, various stabilization theories, including the grain-boundary theory, surface-layer model, domain-wall theory, and volume theory, have been proposed over the past decades (Okasaki & Sakata, 1962; Takahashi, 1970; Carl & Hardtl, 1978; Lambeck & Jonker, 1978; Lambeek & Jonker, 1986; Robels & Arlt, 1993). Among them, the domain-wall-pinning effect has been accepted as a general mechanism of aging (Lambeek & Jonker, 1986; Ren, 2004). It is only quite recently that the volume effect based on the symmetry-conforming principle of point defects was proposed and recognized as the intrinsic governing mechanism of ferroelectric aging (Lambeek & Jonker, 1986; Zhang & Ren, 2006; Yuen et al. 2007).

Compared to tetragonal ferroelectrics, orthorhombic ferroelectrics are as interesting and as important, since orthorhombic ferroelectric phase lies widely in ferroelectrics similar to tetragonal ferroelectric phase (Yamanouchi et al., 1997; Saito et al., 2004; Wang et al., 2006). In particuar, orthorhombic $A^{+}B^{5+}O_3$ alkaline niobates ($KNbO_3$) are promising candidates for

lead-free piezoelectric applications due to their good piezoelectric properties and high Curie temperatures (Yamanouchi et al., 1997; Saito et al., 2004). However, literature report on the aging effects in this class of (lead-free) ferroelectrics remains essentially insufficient till today (Feng & Or, 2009).

More recently, we have investigated the aging effects in an Mn-doped orthorhombic $KNbO_3$-based $[K(Nb_{0.90}Ta_{0.10})O_3]$ lead-free ceramic: $K[(Nb_{0.90}Ta_{0.10})_{0.99}Mn_{0.01}]O_3$ so as to provide a relatively complete picture about the aging on both orthorhombic and tetragonal ferroelectrics for the related communities (Feng & Or, 2009). In this work, we present the aging-induced double P–E loops and recoverable S-E curves in the ceramic, and show that aging in the orthorhombic ferroelectric state is capable of inducing an obvious double P–E loop accompanying a recoverable electrostrain as large as 0.15% at 5 kV/mm at room temperature. Such aging effects are interpreted by a point defect-mediated reversible domain switching mechanism of aging driven by a symmetry-conforming short-range ordering (SC-SRO) of point defects. Large nonlinear electrostrains in excess of 0.13% over a broad temerpature range of 25–140 °C are also demonstrated, suggesting potential application of the aging effects to modify or enhance the electromechanical properties of environmentally-friendly (lead-free) ceramics.

2. Ceramic preparation and property measurements

2.1 Ceramic preparation

The Mn-doped orthorhombic $A^+B^{5+}O_3$ alkaline niobate ($KNbO_3$)-based $[K(Nb_{0.90}Ta_{0.10})O_3]$ lead-free ceramic: $K[(Nb_{0.90}Ta_{0.10})_{0.99}Mn_{0.01}]O_3$ was synthesized using a conventional solid-state reaction technique (Yamanouchi et al., 1997; Saito et al., 2004). The parental compound $K(Nb_{0.90}Ta_{0.10})O_3$ was essentially based on $KNbO_3$ but was modified by adding 10% Ta to the Nb site. As shown in Fig. 1, such modification served to shift the cubic (paraelectric)-tetragonal (ferroelectric) phase transition temperature T_C and the tetragonal (ferroelectric)-orthorhombic (ferroelectric) phase transition temperature $T_{O\text{-}T}$ to the lower temperature side, besides making the "hard" material to be relatively "soft" (Triebwasser, 1959). To formulate the ceramic, 1.0 mol.% Mn was added to the B-site of $K(Nb_{0.90}Ta_{0.10})O_3$ as the acceptor dopant.

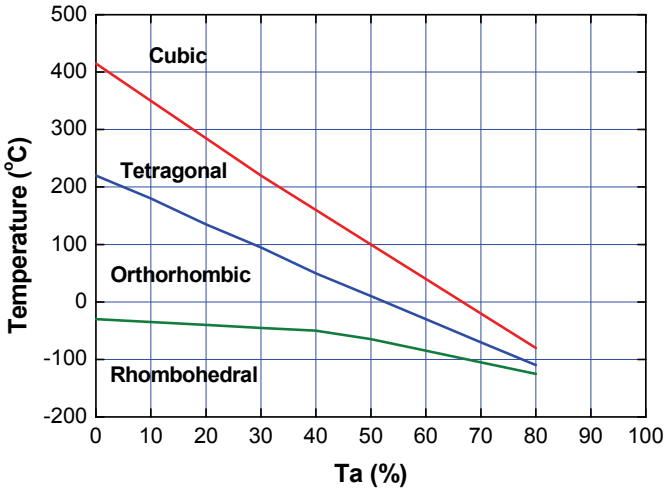

Fig. 1. Phase diagram of $K(Nb_{1-x}Ta_x)O_3$ compound

The starting chemicals were K_2CO_3 (99.5%), Nb_2O_5 (99.9%), Ta_2O_5 (99.9%), and MnO_2 (99%). Calcination was done at 850 °C for 4 h in a K_2O-rich atmosphere, while sintering was carried out at 1050 °C for 0.5 h in air. In order to remove the historical effect, all the as-prepared samples were deaged by holding them at 500 °C for 1 h followed by an air-quench to room temperature. The quenched and deaged samples are designated as "fresh samples". Some fresh samples were aged at 130 °C for 5 days, and the resulting samples are denoted as "aged samples".

2.2 Property measurements

The temperature dependence of dielectric constant of the fresh samples was evaluated at different frequencies using a LCR meter (HIOKI 3532) with a temperature chamber. The bipolar and unipolar ferroelectric hysteresis (*P*–*E*) loops and electrostrain (*S*-*E*) curves for the aged and fresh samples were measured at a frequency of 5 Hz using a precision ferroelectric test system (Radiant Workstation) and a photonic displacement sensor (MTI 2000) under various temperatures in a temperature-controlled silicon oil bath (Fig. 2).

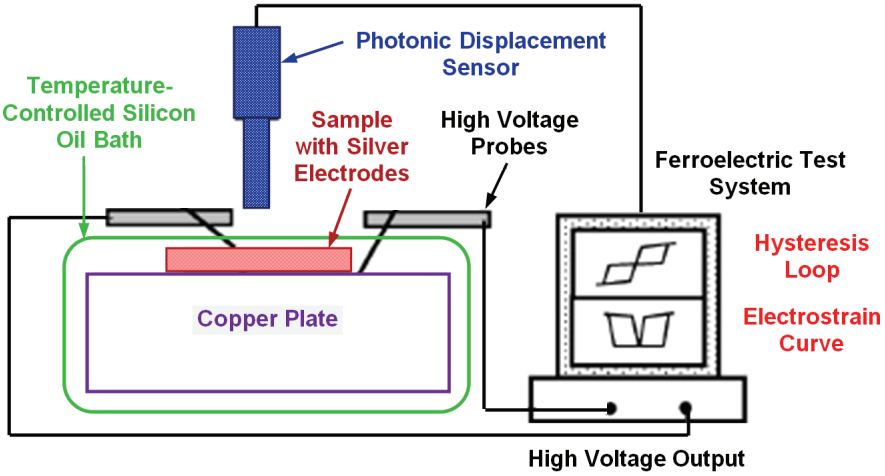

Fig. 2. Experimental setup for measuring bipolar and unipolar ferroelectric hysteresis (*P*–*E*) loops and electrostrain (*S*–*E*) curves

3. Results and discussion

3.1 Temperature dependence of dielectric constant

Fig. 3 shows the temperature dependence of dielectric constant for the fresh samples at three different frequencies of 0.1, 1, and 10 kHz. Three distinct dielectric peaks are observed at about 326, 148, and -15 °C, respectively. X-ray diffraction (XRD) characterization indicates that they correspond to the cubic (paraelectric)-tetragonal (ferroelectric) phase transition temperature T_C, the tetragonal (ferroelectric)-orthorhombic (ferroelectric) phase transition temperature $T_{O\text{-}T}$, and the orthorhombic (ferroelectric)-rhombohedral (ferroelectric) phase transition temperature $T_{R\text{-}O}$, respectively (Triebwasser, 1959). Therefore, our samples have a rhombohedral (*R*) structure for temperatures below -15 °C, an orthorhombic (*O*) structure

for temperatures ranging from -15 to 148 °C, a tetragonal (*T*) structure for temperatures varying from 148 to 326 °C, and a cubic (*C*) structure for temperatures above 326 °C.

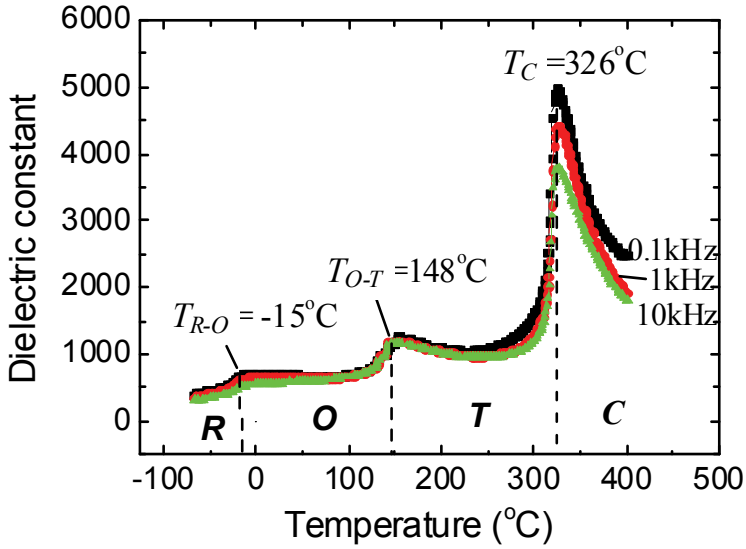

Fig. 3. Temperature dependence of dielectric constant for the fresh samples at three different frequencies of 0.1, 1, and 10 kHz. *C*=cubic, *T*=tetragonal, *O*=orthorhombic, and *R*=rhombohedral

3.2 Room-temperature bipolar and unipolar ferroelectric hysteresis loops and electrostrain curves

Fig. 4 illustrates the bipolar and unipolar ferroelectric hysteresis (*P*–*E*) loops and electrostrain (*S*-*E*) curves for the aged and fresh samples at room temperature. In contrast with the normal bipolar *P*–*E* loop for the fresh samples, the aged samples in Fig. 4(a) possess an interesting bipolar double *P*–*E* loop, very similar to that of the aged acceptor-doped tetragonal ferroelectrics such as the $A^{2+}B^{4+}O_3$ system (Ren, 2004; Zhang & Ren, 2005; Zhang & Ren, 2006). Moreover, a large recoverable electrostrain of 0.15% at 5 kV/mm, accompanying the double *P*–*E* loop, is achieved in our aged samples. This recoverable *S*–*E* curve is indeed different from the butterfly irrecoverable *S*–*E* curve as obtained in the fresh samples due to the existence of a recoverable domain switching in the aged samples but an irrecoverable domain switching in the fresh samples. Fig. 4(b) shows the unipolar *P*–*E* loops and *S*–*E* curves for the aged and fresh samples. It is clear that a large polarization *P* of about 22 μC/cm² is obtained at 5 kV/mm for the aged samples compared to a much smaller *P* of about 6 μC/cm² in the fresh samples at the same field level. With the large *P*, a large nonlinear electrostrain of 0.15% at 5 kV/mm is available for the aged samples owing to the reversible domain switching. It is noted that this electrostrain not only is 2.5 times larger than the fresh samples, but also exceeds the "hard" lead zirconate titanate (PZT) value of 0.125% at 5 kV/mm (Park & Shrout, 1997). It is also noted that the electrostrain in our fresh

samples (having a small quantity of Mn acceptor dopant) is not obviously different from that in the undoped $K(Nb_{0.90}Ta_{0.10})O_3$ ceramic, and similarly large electrostrain has been reported recently on the aged tetragonal $K(Nb_{0.65}Ta_{0.35})O_3$-based ceramics (Feng & Ren, 2007).

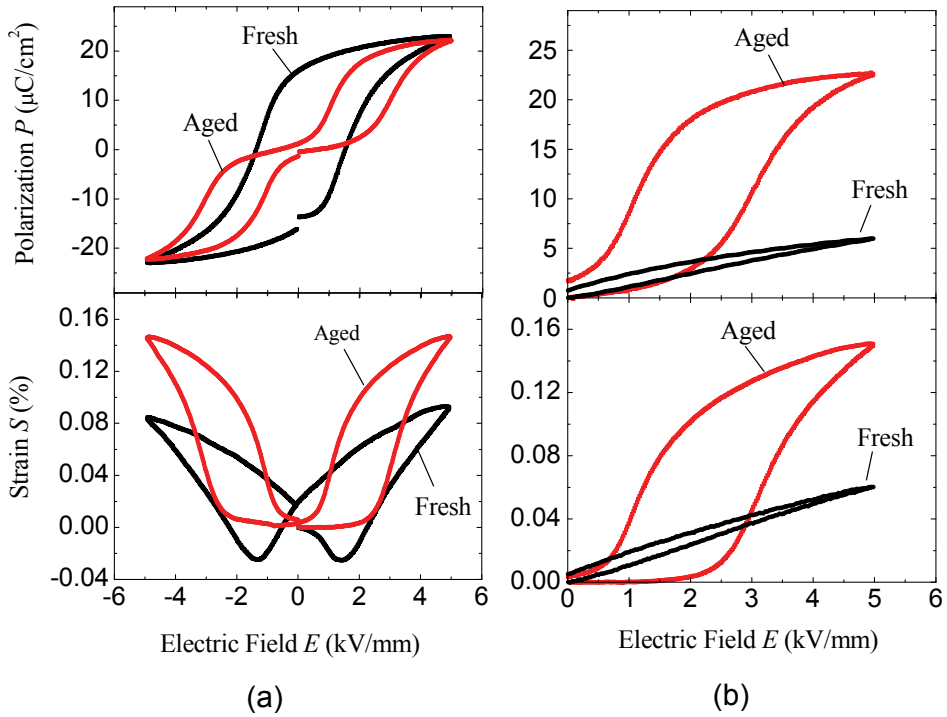

Fig. 4. (a) Bipolar and (b) unipolar ferroelectric hysteresis (*P*–*E*) loops and electrostrain (*S*-*E*) curves for the aged and fresh samples at room temperature

3.3 Physical interpretation by a point defect-mediated reversible domain switching mechanism of aging

Although our orthorhombic $K[(Nb_{0.90}Ta_{0.10})_{0.99}Mn_{0.01}]O_3$ ceramic has different crystal symmetry from tetragonal ferroelectric $BaTiO_3$, they all belong to perovskite ABO_3 structure. This lets us to believe that the observed aging effects in our aged orthorhombic samples can be explained according to a point defect-mediated reversible domain switching mechanism of aging driven by a symmetry-conforming short-range ordering (SC-SRO) of point defects (i.e., acceptor ions and vacancies) adopted successfully in $BaTiO_3$ (Ren, 2004; Zhang & Ren, 2005; Zhang & Ren, 2006). In fact, when acceptor dopant Mn^{4+}/Mn^{3+} ions displace the central Nb^{5+}/Ta^{5+} ions of the *B*-site in the aged $K[(Nb_{0.90}Ta_{0.10})_{0.99}Mn_{0.01}]O_3$ samples, oxygen vacancies V_O form at the O^{2-} sites to maintain the charge neutrality, resulting in point defects (i.e., defect dipoles) with the central acceptor dopants. Fig. 5 depicts how such aging effects are produced in a single-crystal grain of our aged samples. Some associated remarks are included as follows.

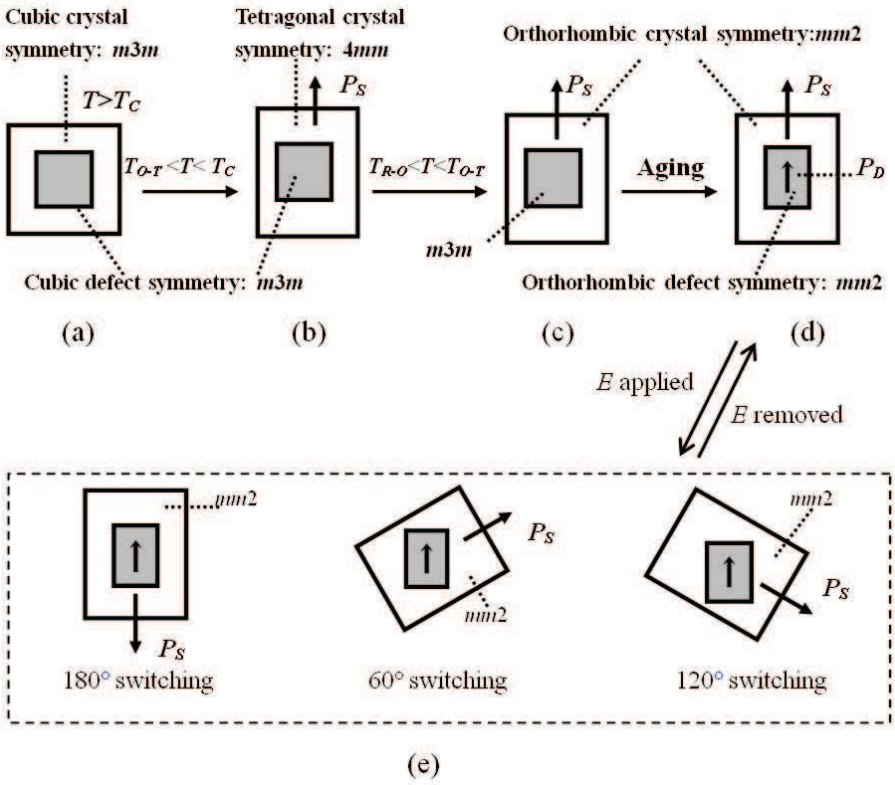

Fig. 5. Crystal and defect symmetries of a single-crystal grain in (a) a fresh $K[(Nb_{0.90}Ta_{0.10})_{0.99}Mn_{0.01}]O_3$ sample at $T>T_C$, (b) the fresh sample at $T_{O\text{-}T}<T<T_C$, (c) the fresh sample at $T_{R\text{-}O}<T<T_{O\text{-}T}$, and (d) an aged sample at room temperature. (e) Electric field *E*-induced switching of the 180°, 60°, and 120° ferroelectric domains in the aged sample at room temperature

1. When the fresh samples are just sintered and their temperature T is still above the Curie point T_C (i.e., $T>T_C$), its single-crystal grain exhibits a cubic crystal symmetry *m*3*m*, and point defects naturally show a conforming cubic defect symmetry *m*3*m*, as shown in Fig. 5(a).
2. At $T_{O\text{-}T}<T<T_C$, the single-crystal grain of the fresh samples shows a tetragonal crystal symmetry 4*mm*, due to the displacement of positive and negative ions along the [001] crystallographic axis, producing a nonzero spontaneous polarization P_S as shown in Fig. 5(b). However, the short-range ordering (SRO) distribution of point defects keeps the same cubic defect symmetry *m*3*m* as that in the cubic paraelectric phase because the diffusionless paraferroelectric transition cannot alter the original cubic SRO symmetry of point defects (Ren, 2004).
3. At $T_{R\text{-}O}<T<T_{O\text{-}T}$, the single-crystal grain of the fresh samples exhibits an orthorhombic crystal symmetry *mm*2, owing to the ferroelectric-ferroelectric phase transition from the tetragonal to orthorhombic structure, producing a nonzero P_S along the [110]

crystallographic axis as shown in Fig. 5(c). Again, the SRO distribution of point defects still keeps the same cubic defect symmetry *m*3*m* because of fast cooling. As a result, two unmatched symmetries (i.e., the orthorhombic crystal symmetry and the cubic defect symmetry) exist simultaneously in the fresh ferroelectric state [Fig. 5(c)]. According to the SC-SRO principle (Ren & Otsuka, 2000), such a state is energetically unstable and the samples tend to a symmetry-conforming state.

4. After aging at 130 °C for 5 days in the ferroelectric state, the cubic defect symmetry *m*3*m* changes gradually into a polar orthorhombic defect symmetry *mm*2, while the single-crystal grain of the aged samples has a polar orthorhombic crystal symmetry *mm*2, as shown in Fig. 5(d). Such a change is realized by the migration of V_O during aging, and the polar orthorhombic defect symmetry creates a defect polarization P_D, aligning along the spontaneous polarization P_S direction [Fig. 5(d)].
5. When an electric field E is initially applied in opposition to P_S of the aged orthorhombic samples [Fig. 5(e)], an effective switching of the available 180° ferroelectric domains is induced, contributing to a small polarization at low E (<1.5 kV/mm), as shown in Fig. 4(b). Continuing a larger applied E (>1.5 kV/mm), non-180° domain switching (mainly 60° and 120° domain switching according to the polar orthorhombic crystal symmetry) is induced, but the polar orthorhombic defect symmetry and the associated P_D cannot have a sudden change [Fig. 5(e)]. Hence, the unchanged defect symmetry and the associated P_D cause a reversible domain switching after removing E. Consequently, an interesting macroscopic double P–E loop and a large recoverable S–E curve are produced as in Fig. 4. For the fresh samples, since the defect symmetry is a cubic symmetry and cannot provide such an intrinsic restoring force, we can only observe a normal macroscopic P–E loop and a butterfly S–E curve due to the irreversible domain switching [Fig. 4(a)].

It should be noted that the microscopic description for the orthorhombic $KNbO_3$-based ferroelectrics is very similar to that for acceptor-doped tetragonal ferroelectric titanates (Ren, 2004; Zhang & Ren, 2005; Zhang & Ren, 2006). The observed aging effects originate essentially from the inconformity of the crystal symmetry with the defect symmetry after a structural transition. This may be the intrinsic reason why macroscopic double P-E loops and recoverable S–E curves are achieved in different ferroelectric phases and different ferroelectrics. Such aging mechanism, based on the SC-SRO principle of point defects, is insensitive to crystal symmetry and constituent ionic species, indicating a common physical origin of aging.

3.4 Effect of temperature on ferroelectric hysteresis loops and electrostrain curves

Fig. 6 plots the unipolar ferroelectric hysteresis (P–E) loops and electrostrain (S–E) curves for the aged samples at five different temperatures of 25, 80, 120, 140, and 160 °C in order to investigate their temperature stabilities for applications. The insets show the temperature dependence of maximum polarization P_{max} and maximum strain S_{max} of the aged samples at 5 kV/mm. It can be seen that the aging-induced high P_{max} in excess of 19 μC/cm² and large S_{max} in excess of 0.13% can be persisted up to 140 °C, reflecting a good temperature stability for the effects. Above 140 °C, both the unipolar P–E loop and S–E curve become normal, while P_{max} and S_{max} decrease significantly. This can be ascribed to the destruction of defect symmetry and migration of V_O as a result of the exposure to high temperature and the approach of the tetragonal phase ($T_{O\text{-}T}$ =148 °C). Thus, point defects cannot provide a

restoring force for a reversible domain switching so that the obvious *P*–*E* loop becomes a normal loop and the recoverable *S*–*E* curve vanishes.

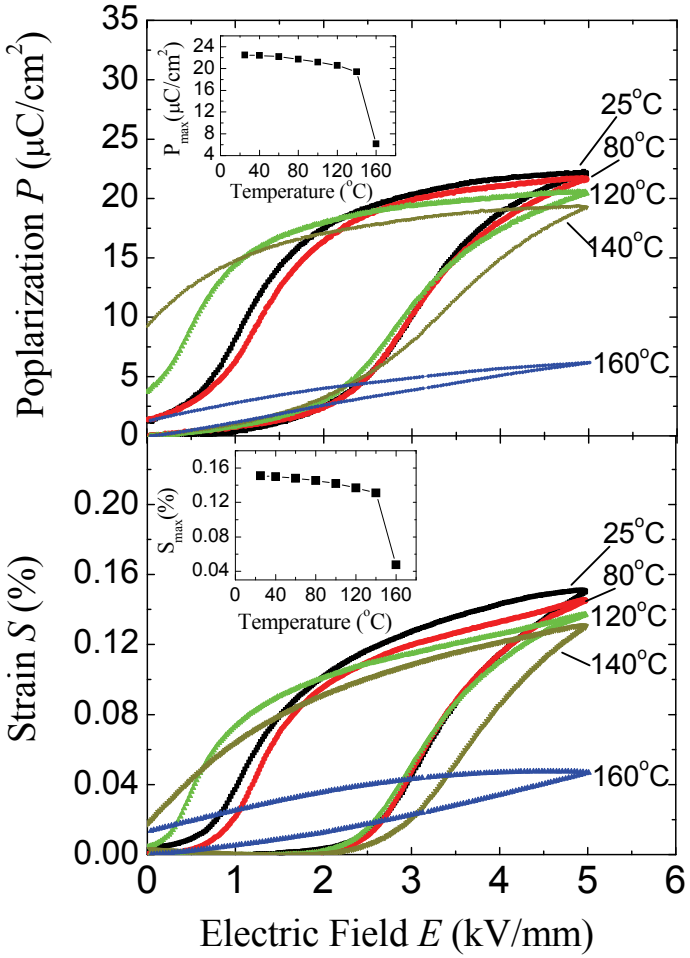

Fig. 6. Unipolar ferroelectric hysteresis (*P*–*E*) loops and electrostrain (*S*–*E*) curves for the aged samples at five different temperatures of 25, 80, 120, 140, and 160 °C. The insets show the temperature dependence of maximum polarization P_{max} and maximum strain S_{max} of the aged samples at 5 kV/mm

4. Conclusion

In summary, we have investigated the aging-induced double ferroelectric hysteresis (*P*–*E*) loops and recoverable electrostrain (*S*–*E*) curves in an Mn-doped orthorhombic $KNbO_3$-based $[K(Nb_{0.90}Ta_{0.10})O_3]$ lead-free ceramic: $K[(Nb_{0.90}Ta_{0.10})_{0.99}Mn_{0.01}]O_3$. Obvious double *P*–*E*

loops and large recoverable *S*–*E* curves with amplitudes in excess of 0.13% at 5 kV/mm have been observed in the aged samples over a wide temperature range of 25–140 °C. The observations have been found to have striking similarities to tetragonal ferroelectrics, besides following a point defect-mediated reversible domain switching mechanism of aging driven by a symmetry-conforming short-range ordering (SC-SRO) of point defects. Such aging effects, being insensitive to crystal structure and constituent ionic species, provide a useful way to modify or enhance the electromechanical properties of lead-free ferroelectric material systems.

5. Acknowledgements

This work was supported by the Research Grants Council and the Innovation and Technology Fund of the Hong Kong Special Administration Region (HKSAR) Government under Grant Nos PolyU 5266/08E and GHP/003/06, respectively.

6. References

Arlt, G. & Rebels U. (1993). Aging and fatigue in bulk ferroelectric perovskite ceramics. *Integrated Ferroelectrics*, 3, 343–349

Carl, K. & Hardtl, K. H. (1977). Electrical after-effects in Pb(Ti, Zr)O_3 ceramics. *Ferroelectrics*, 17, 473-486

Damjanovic, D. (1998). Ferroelectric, dielectric and piezoelectric properties of ferroelectric thin films and ceramics. *Reports on Progress in Physics*, 61, 1267-1324

Feng, Z. Y. & Ren, X. (2007). Aging effect and large recoverable electrostrain in Mn-doped $KNbO_3$-based ferroelectrics. *Applied Physics Letters*, 91, 032904

Feng, Z. Y. & Or, S. W. (2009). Aging-induced, defect-mediated double ferroelectric hysteresis loops and large recoverable electrostrains in Mn-doped orthorhombic $KNbO_3$-based ceramics. *Journal of Alloys and Compounds*, 480, L29-L32

Hall, D. A. & Ben-Omran, M. M. (1998). Ageing of high field dielectric properties in $BaTiO_3$-based piezoceramics. *Journal of Physics: Condensed Matter*, 10, 9129–9140

Jaffe, B.; Cook, W. R. & Jaffe, H. (1971). *Piezoelectric Ceramics*, Academic Press, 0123795508, New York

Lambeck, P. V. & Jonker, G. H. (1978). Ferroelectric domain stabilization in $BaTiO_3$ by bulk ordering of defects. *Ferroelectrics*, 22, 729-731

Lambeek, P. V. & Jonker, G. H. (1986). The nature of domain stabilization in ferroelectric perovskites. *Journal of Physics and Chemetry of Solids*, 47, 453–461

Okasaki, K. & Sakata, K. (1962). Space charge polarization and aging of barium titanate ceramics. *Electrotechnical Journal of Japan*, 7, 13–18

Park, S. -E. & Shrout, T. R. (1997). Ultrahigh strain and piezoelectric behavior in relaxor based ferroelectric single crystals. *Journal of Applied Physics*, 82, 1804-1811

Ren, X. & Otsuka, K. (2000), Universal symmetry property of point defects in crystals. *Physical Review Letters*, 85, 1016–1019

Ren, X. (2004). Large electric-field-induced strain in ferroelectric crystals by point-defect-mediated reversible domain switching. *Nature Materials*, 3, 91–94

Robels, U. & Arlt, G. (1993). Domain wall clamping in ferroelectrics by orientation of defects. *Journal of Applied Physics*, 73, 3454-3460

Schulze, W. A. & Ogino, K. (1988). Review of literature on aging of dielectrics. *Ferroelectrics*, 87, 361–377

Takahashi, M. (1970). Space charge effect in lead zirconate titanate ceramics caused by the addition of impurities. *Japnese Journal of Applied Physics*, 9, 1236–1246

Triebwasser, S. (1959). Study of ferroelectric transitions of solid-solution single crystals of $KNbO_3$-$KTaO_3$. *Physical Review*, 114, 63–70

Uchino, K. (2000). *Ferroelectric Device*, Mercel Dekker, Inc., 0-8247-8133-3, New York

Wang, X. X.; Or, S. W.; Lam, K. H.; Chan, H. L. W.; Choy, P. K. & Liu, P. C. K. (2006). Cymbal actuator fabricated using $(Na_{0.46}K_{0.46}Li_{0.08})NbO_3$ lead-free piezoceramic. *Journal of Electroceramics*, 16, 385–388

Yamanouchi, K.; Odagawa, H.; Kojima, T. & Matsumura, T. (1997). *Electronic Letters*, 33, 193
Saito, Y.; Takao, H.; Tani, T.; Nonoyama, T.; Takatori, K.; Homma, T.; Nagaya, T. & Nakamura, M. (2004). Lead free Piezoceramics. *Nature*, 432, 84–87

Yuen, G. L.; Yang, Y. & Or, S. W. (2007). Aging-induced double ferroelectric hysteresis loops in $BiFeO_3$ multiferroic ceramic. *Applied Physics Letters*, 91, 122907

Zhang, L. X. & Ren, X. (2005). *In situ* observation of reversible domain switching in aged Mn-doped $BaTiO_3$ single crystals. *Physical Revuew B*, 71, 174108

Zhang, L. X. & Ren, X. (2006). Aging behavior in single-domain Mn-doped $BaTiO_3$ crystals: Implication for a unified microscopic explanation of ferroelectric aging. *Physical Revuew B*, 73, 094121

Ferroelectrics

Edited by Dr Indrani Coondoo

ISBN 978-953-307-439-9
Hard cover, 450 pages
Publisher InTech
Published online 14, December, 2010
Published in print edition December, 2010

Ferroelectric materials exhibit a wide spectrum of functional properties, including switchable polarization, piezoelectricity, high non-linear optical activity, pyroelectricity, and non-linear dielectric behaviour. These properties are crucial for application in electronic devices such as sensors, microactuators, infrared detectors, microwave phase filters and, non-volatile memories. This unique combination of properties of ferroelectric materials has attracted researchers and engineers for a long time. This book reviews a wide range of diverse topics related to the phenomenon of ferroelectricity (in the bulk as well as thin film form) and provides a forum for scientists, engineers, and students working in this field. The present book containing 24 chapters is a result of contributions of experts from international scientific community working in different aspects of ferroelectricity related to experimental and theoretical work aimed at the understanding of ferroelectricity and their utilization in devices. It provides an up-to-date insightful coverage to the recent advances in the synthesis, characterization, functional properties and potential device applications in specialized areas.

How to reference

In order to correctly reference this scholarly work, feel free to copy and paste the following:

Siu Wing Or (2010). Aging-Induced, Defect-Mediated Double Ferroelectric Hysteresis Loops and Large Recoverable Electrostrains in Mn-Doped Orthorhombic KNbO3-Based Lead-Free Ceramics, Ferroelectrics, Dr Indrani Coondoo (Ed.), ISBN: 978-953-307-439-9, InTech, Available from: http://www.intechopen.com/books/ferroelectrics/aging-induced-defect-mediated-double-ferroelectric-hysteresis-loops-and-large-recoverable-electrostr

INTECH
open science | open minds

InTech Europe
University Campus STeP Ri
Slavka Krautzeka 83/A
51000 Rijeka, Croatia
Phone: +385 (51) 770 447
Fax: +385 (51) 686 166
www.intechopen.com

InTech China
Unit 405, Office Block, Hotel Equatorial Shanghai
No.65, Yan An Road (West), Shanghai, 200040, China
中国上海市延安西路65号上海国际贵都大饭店办公楼405单元
Phone: +86-21-62489820
Fax: +86-21-62489821